CrystEngComm

Accepted Manuscript

ROYAL SOCIETY OF CHEMISTRY

www.rsc.org/crystengcomm

CrystEngComm

ARTICLE

Transformation of Amorphous Calcium Carbonate Nanoparticles into Aragonite Controlled by ACCBP

Received 00th January 20xx,
Accepted 00th January 20xx

DOI: 10.1039/x0xx00000x

www.rsc.org/

Jingtan Su,[a] Fangjie Zhu,[a] Guiyou Zhang,[a] Hongzhong Wang,[a] Liping Xie*[, a] and Rongqing Zhang*[, a, b]

Polymorph selection during shell or pearl formation has been an intriguing issue, especially for those species of interest of human consumption. The polymorph switching of calcium carbonate controlled by amorphous calcium carbonate-binding protein (ACCBP), an extrapallial fluid (EPF) protein of pearl oyster identified by our group in 2007, is investigated in this research. FTIR and TGA analysis suggest that ACCBP decreases the bound water content of amorphous calcium carbonate (ACC), suggesting that ACCBP may be involved in biogenic anhydrous ACC formation. I*n vitro* crystallization and ACC transformation experiments show that ACCBP induces aragonite formation via ACC precursor in Mg/Ca = 1 and Mg/Ca = 2 solutions at low temperature. Raman, FTIR, ICP and XPS analyses of the initial-stage ACC nanoparticles in the ACC transformation experiment suggest that this polymorph switching may be controlled by increasing the surface Mg/Ca ratio of ACC, rather than by regulating the bulk Mg/Ca ratio or the short-range ordered structure. These results suggest that the polymorph selection in nacre or pearl growth may be controlled not only by the nucleating template on the matrix but also by the physicochemical effects of EPF proteins.

Introduction

Shell of many mollusks such as the pearl oyster, *Pinctada fucata*, comprises two distinct layers of calcium carbonate known as the nacre (aragonite) and prism (calcite). It has a highly organized hierarchical structure over several length scales and exhibits superior mechanical properties.[1-3] For example, the toughness of nacre is approximately 3,000-fold greater than that of pure aragonite, which constitutes 95% of nacre.[4] The synthesis of this amazing biomineral occurs in a mild condition under the control of biomolecules,[5] and it happens via amorphous calcium carbonate (ACC) precursor.[6-10] According to a recent model, ACC precursor forms by aggregation of prenucleated ion clusters,[11, 12] and is stabilized by Mg^{2+}, phosphate or biomolecules.[13-17] This amorphous precursor is then transported to the final mineralization site, where it is destabilized by Asp-rich protein and crystallized into aragonite or calcite.[18, 19]

The polymorph of calcium carbonate during shell of pearl formation is supposed to be determined by an epitaxial match between the formed mineral and the supramolecular template matrix. This template is a highly ordered composite of crystal-nucleating acidic proteins and structural framework macromolecules (mostly chitin).[3, 20] Indeed, a zone rich in carboxylates surrounded by a ring rich in sulfates has been found on the matrix surface underlying the centre of each aragonitic tablet in nacre, and polyclonal antibodies raised against the aragonite-nucleating macromolecule fraction suggest that this zone is a nucleation site for aragonite.[21] Extensive studies on the matrix of nacre demonstrate that a combination of β-chitin, silk fibrin and glycoproteins is responsible for the formation of the aragonite mineral phase.[3, 13, 22-24] Particularly, AP7, N40 and PFMG1 nucleate aragonite in solution without any additives such as Mg^{2+}.[25-28] N16, an intrinsically disordered oligomeric nacre framework protein, nucleates vaterite and single crystal aragonite.[29, 30] N16 and Pif80/Pif97 assemble with β-chitin to form lamellar framework nucleation sheets or films within nacre, to induce aragonite formation and to control crystal orientation.[23, 24, 31] Furthermore, K58, a matrix protein from bivalve ligament, induces aragonite formation with unusual morphologies via ACC precursor, which also supports this epitaxial match theory.[32]

Some investigations of the structure of nacre provide evidences against this epitaxial match theory. Nassif *et al*. revealed that the aragonitic tablets in nacre are covered with a continuous layer of ACC and there was no protein interaction with this layer.[33] Rousseau *et al*. revealed that each aragonitic tablet is divided into nanograins by a continuous organic framework.[2] Li *et al*. confirmed that a single-crystal-like aragonitic tablet was essentially assembled with aragonite nanograins and amorphous phase was found between them.[34] These findings imply that aragonite mineral phase forms

[a] *Institute of Marine Biotechnology, School of Life Sciences, Tsinghua University, Beijing 100084, China.*
E-mail: rqzhang@mail.tsinghua.edu.cn or lpxie@mail.tsinghua.edu.cn
[b] *Protein Science Laboratory of the Ministry of Education, Tsinghua University, Beijing 10084, China.*

† Footnotes relating to the title and/or authors should appear here.
Electronic Supplementary Information (ESI) available: [details of any supplementary information available should be included here]. See DOI: 10.1039/x0xx00000x

directly from ACC nanograins transformation without the control of the nucleating template on the matrix. These investigations reemphasize that the mechanisms by which the amorphous phase is switched into a specific calcium carbonate polymorph are still largely unclear, and that the polymorph may be controlled by some indispensable factors besides the nucleating template.

Amorphous calcium carbonate-binding protein (ACCBP) is an extrapallial fluid (EPF) protein identified by our group in 2007.[35] It mainly stays in hemolymph and EPF and can be detected by western-blot in neither EDTA-soluble shell matrix nor EDTA-insoluble shell matrix.[35] It is expressed by mantle cells which are responsible for shell formation,[36] participates in ACC formation and stabilization, and controls the morphology of the nacre layer in mature shell.[35] The 5-fold symmetry of its Ca^{2+}-binding sites is the structural basis for this function.[37] The partially disordered N-terminal sequence and the acetylcholine binding sites are important for the mineralization activity.[38, 39] ACCBP is expressed in the pearl sac during the early stage of pearl formation. Real-time PCR shows that the expression level of ACCBP reaches a maximum at the 30th day when a thin layer of ACC covers the implanted aragonitic nuclei, and decreases significantly after the first nacreous layer has formed.[40] During the formation of a flat pearl, ACCBP expression is detected in the mantle. RT-PCR shows that the expression of ACCBP holds comparatively steady from day 15 to 25 in both the inner-film and film-free system during the formation of nacreous layer.[41] Recent report shows that once EPF was extracted daily for 20 days, the nacre platelet in the nacreous layer is disturbed, and calcite deposited randomly.[42] Similar to Pif 97 (14.5 Asp, 6.5% Glu), ACCBP is rich in Asp (10.0%) and Glu (4.6%) and its calculated isoelectric point is 4.72. Considering that acidic proteins are associated with polymorph regulation and that the poly-(Asp) can induce aragonite formation,[23, 43, 44] it's reasonable to assume that ACCBP may be involved in polymorph selection, and it's interesting to study whether and how ACCBP, which is not a template matrix protein, controls the polymorph selection during ACC crystallization.

In the present work, two different precipitation experiments with or without ACCBP were conducted, and the characteristics of the initial-stage precipitate from the ACC transformation experiment was investigated. The results show that ACCBP decreases the water content of ACC, that ACCBP induces the formation of aragonite via ACC precursor in Mg/Ca = 1 and Mg/Ca = 2 solution even at low temperature, and that ACCBP may recruit Mg^{2+} onto the surface of ACC. These results are consistent with the hints of *in vivo* studies, suggesting that polymorph selection during nacre growth is controlled not only by the nucleating template on the matrix but also by the physicochemical effects of extrapallial proteins.

Experimental

Protein expression, purification and activity analysis. The expression plasmid was constructed by inserting the ACCBP gene into the vector pET21b, which was then transferred into *E. coli*. (OrigamiTM B). The expression host was incubated at 37°C in LB medium containing ampicillin. When the OD_{600} of the culture reached 0.6, the temperature was reduced to 8°C, and protein expression was induced by adding 0.1 mM IPTG, 1.0% glycerol, and 1 mM $CaCl_2$. After 48 hr of induction, the cells were harvested by centrifugation at 8000 × g for 6 min at 4°C. The harvested cells were re-suspended and subjected to ultrasonication, and the protein was purified using Ni^{2+}-NTA affinity chromatography. The protein was desalted using a HisTrapTM Desalting column and was kept at 4°C before use. The protein concentration was determined by the absorbance at 280 nm using ε280nm = 42,400 $M^{-1}cm^{-1}$. The activity of recombinant ACCBP was detected following the methods of Su *et al*.[37]

I*n vitro* crystallization experiment. This experiment was adapted from the method described by Xu *et al*.[45] A saturated $Ca(HCO_3)_2$ solution was prepared by bubbling CO_2 gas into Milli-Q water in the presence of calcium carbonate for 4 hr. Excess solid calcium carbonate was removed by filtration. The final concentration of calcium was 8.5 mM, as determined by EDTA titration. The freshly prepared $Ca(HCO_3)_2$ was immediately mixed with various amounts of ACCBP and $MgCl_2$ to prepare a number of samples. The same concentrations of bovine serum albumin (BSA) were used instead in the control experiments. The final concentration of $Ca(HCO_3)_2$ in the mixed solutions was approximately 8.0 mM, the concentration of ACCBP was 0.5 μM, and the concentrations of $MgCl_2$ were 0, 8.0 and 16.0 mM (Mg/Ca ratios of 0, 1 and 2, respectively). Hydrophobic glass slides placed in 6-well COSMO multidishes were then treated with 20 μl of the mixed solutions, and 20 μl of a 1 M NaOH solution was added to the bottom of each well to absorb the CO_2 diffusing from the mixed solution. The samples were kept in a laboratory refrigerator (MPR 1410, SANYO) being set at 6°C. After 24 hr, the drops were absorbed with Waterman filter paper. The crystals left on the slides were investigated using SEM and Raman spectroscopy *in situ*.

ACC transformation experiment. This experiment was adapted from the method described by Koga *et al*.[46] The 50 mM $CaCl_2$ solutions were prepared with Mg/Ca ratios of 1 and 2, with or without 0.5 μM ACCBP. The 50 mM $CaCl_2$ solution was then added to the 50 mM Na_2CO_3 solution, and mixed evenly. The freshly synthesized ACC samples were kept in the solutions in a laboratory refrigerator (MPR 1410, SANYO) being set at 6°C. The calcium carbonate precipitates were collected at 0, 12, 24, 48, and 72 hr for FTIR, micro-Raman, SEM, DSC, ICP and XPS analysis, and were collected at 96 hr for XRD analysis. ACC transformation experiment and *in vitro* crystallization experiment were conducted to investigate the function of ACCBP in different precipitation systems.

Polymorph analysis (XRD, FTIR, micro-Raman). XRD data was collected using a D/max 2500 X-ray diffractometer with Cu Kα radiation at 50 kV and 200 mA. Samples were scanned between 2θ values of 10° and 90° at a scan speed of 1.2 °/min. The aragonite content in the calcium carbonate precipitates was calculated using the K-value method[47]. The FTIR spectra were collected in the range of 400-4000 cm^{-1} using a Nicolet 560 Fourier transform infrared spectrometer. The Raman spectra were collected using an RM2000 spectrometer with an

excitation wavelength of 514 nm, which was provided by an argon laser set to 4.6 mW. The spectra were collected in the range of 100-1500 cm^{-1}. Each Raman spectral profile represents the average of 6-10 separate scans of the sample.

Elemental analysis (ICP-AES/XPS). The bulk Mg/Ca ratios of the ACC samples were determined using inductively coupled plasma (ICP) spectrometry (VISTA-MPX) with samples dissolved in hydrochloric acid. The surface Mg/Ca ratios of ACC samples at depths less than 5 nm were determined using X-ray photoelectron spectroscopy (XPS). The PHI-5300 Quantera XPS spectrometer (ULVAC-PHI) was equipped with a spherical sector analyzer and an Al Kα X-ray source at 1486.7 nm. Spectra were obtained in a vacuum below 10-8 torr at a detection angle of 45° (relative to the surface). Adventitious carbon, which appears at a binding energy of 284.8 eV on clean metal surfaces, was used as an internal standard to perform charge correction on all samples.

Fluorescence quenching experiment. These experiments were performed using 5 μM ACCBP. The fluorescence spectra were collected using a Hitachi F-2500 spectrofluorometer with a 1-cm-path-length cell and an excitation wavelength of 280 nm.

Themogravimetric Analysis (TGA). The ACC samples were prepared in the presence of 0.0, 0.25, 0.50 and 1.0 μM ACCBP. The bound water content was analyzed using a thermogravimetric analyzer (Q5000). The measurements were performed under nitrogen flow (25 ml/min), with heating from ambient temperature to 900°C at a rate of 10 °C/min.

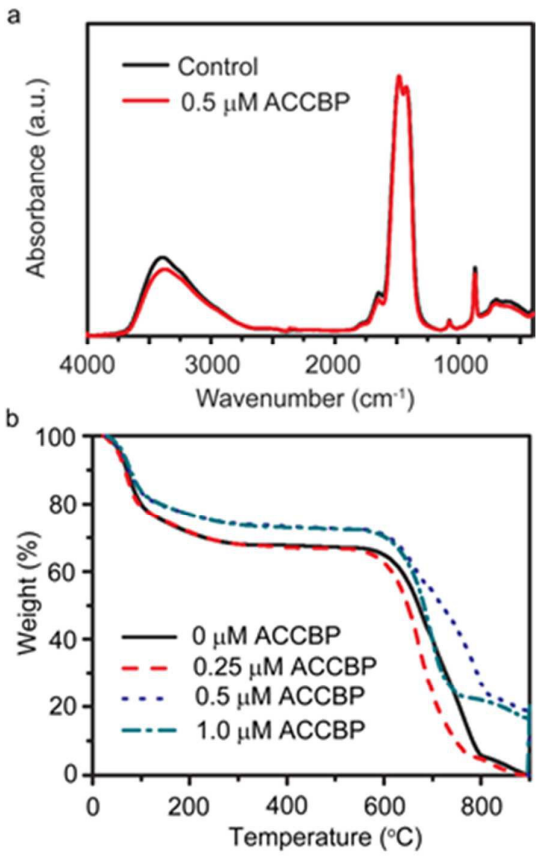

Fig. 1 FTIR spectra a) and TGA b) of ACC prepared in solution with and without ACCBP.

Results

ACCBP induces less hydrated ACC formation. The FTIR spectra of ACC collected at 0 hr in ACC transformation experiment show that ACCBP decreases the 3400 cm^{-1}/866 cm^{-1} intensity ratio (Fig. 1a), implying that ACCBP may decrease the bound water content. ACC prepared with different concentrations of ACCBP is further analysed by TGA (Fig. 1b). According to the thermal behaviour of ACC measured by DSC (Fig. S1) and the data in previous reports,[46, 48, 49] the weight loss below 100°C in TGA is attributed to the release of free water, the loss above 100°C is attributed to the release of bound water, and the loss at approximately 690°C is attributed to the decomposition of calcium carbonate. The weight loss (ΔW) between 100°C and 350°C is considered as the total weight of bound water in the ACC sample, and the weight (W) at approximately 350°C is considered as the total weight of calcium carbonate in the ACC sample. As the molar masses of calcium carbonate and H_2O are 100 g/mol and 18 g/mol, respectively, the bound water content per mol calcium carbonate could be calculated by ΔW×100/(W×18). The results show that the sample prepared without protein contains 1.0 mol of water per mol of calcium carbonate. The addition of 0.25 μM ACCBP does not change the water content of the ACC, while the presence of 0.5 μM and 1 μM ACCBP decrease the water content to 0.82 mol of water per mol of calcium carbonate. The biogenic anhydrous ACC is essentially anhydrous, while the biogenic stable ACC contains 1 mol of bound water per mol of calcium carbonate.[15, 50] ACCBP decreases the bound water content of ACC and may be involved in the formation of biogenic anhydrous ACC *in vivo*.

ACCBP induces aragonite formation via an ACC precursor in low-Mg/Ca solutions at low temperature. The *in vitro* crystallization experiment is conducted at 6°C to avoid protein denaturation or degradation (Fig. 2). An SEM equipped with an energy dispersive spectrometer (EDS) is used to observe the morphology of the precipitates, and Raman spectroscopy is used to characterize the polymorph. ACC is identified by a broad peak at ~1085 cm^{-1}, vaterite by peaks at ~1074 and 1090 cm^{-1}, aragonite by peaks at ~155, ~204, and ~1085 cm^{-1}, and calcite by peaks at ~154, ~281, and ~1085 cm^{-1}.[51, 52] The SEM and Raman results show that ACC spherulites (approximately 9.5 μm in diameter) form in the presence of ACCBP, while only calcite particles form in the control experiment (Fig. 2a&b). The addition of Mg^{2+} dramatically alters the result. Calcite particles and some aragonite particles form instead of ACC spherulites in the solution with an Mg/Ca molar ratio of 1 (Mg/Ca = 1) and ACCBP, while only calcite particles are observed in the control experiment (Fig. 2c&d). More aragonite particles are found in the solution with Mg/Ca = 2 and ACCBP (Fig. 2e&f). Mg^{2+} is an excellent stabilizer of ACC,[14] and calcite is favoured in solution with an Mg/Ca molar ratio

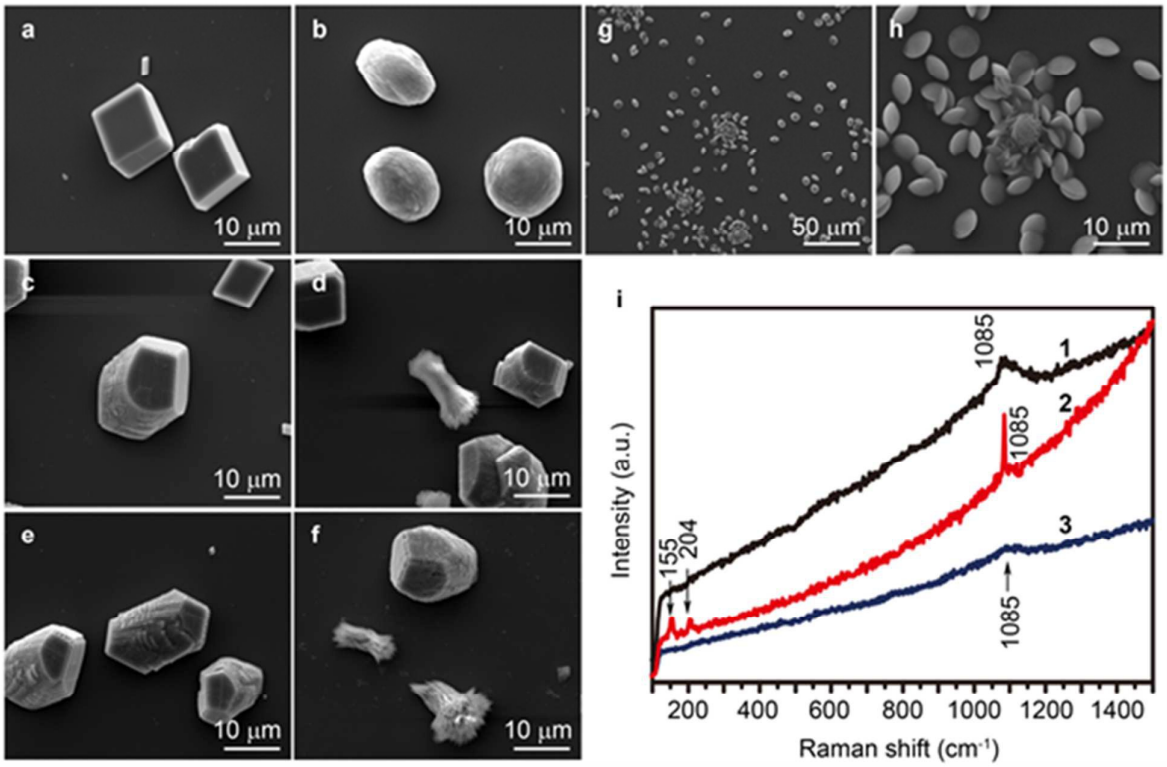

Fig. 2 The *in vitro* crystallization experiment. SEM images of Calcium carbonate precipitates grown for 24 hr in the following solution conditions: a) 0.5 μM BSA, b) 0.5 μM ACCBP, c) Mg/Ca = 1 and 0.5 μM BSA, d) Mg/Ca = 1 and 0.5 μM ACCBP, e) Mg/Ca = 2 and 0.5 μM BSA, f) Mg/Ca = 2 and 0.5 μM ACCBP. g) SEM image of Calcium carbonate precipitates grown for 4 hr in solution with Mg/Ca = 1 and 0.5 μM ACCBP. h) Enlargement of the central region in g. i) Raman spectra of the Calcium carbonate precipitates. Spectrum 1 is from an ACC spherulite in b, spectrum 2 is from an aragonite particle in d, and spectrum 3 is from an ACC spherulite in h.

below 4 at a temperature of 6°C.[53] Therefore, it is unexpected that ACC disappears and aragonite forms in the presence of both ACCBP and Mg.

EDS shows that calcite that grows in the solution with Mg/Ca = 1 and ACCBP has higher magnesian content with an average of 36.4±7.4 mol% for 15 randomly selected particles, compared to 27.9±3.0 mol% for 10 randomly selected calcite particles in the control experiment (data not shown). Considering that high-magnesian calcites can be formed *in vitro* via ACC precursors,[54] the aragonites in Mg/Ca = 1 and Mg/Ca = 2 solutions may form by consuming the ACC precursor under the control of ACCBP.

Investigations of the early-stage samples of *in vitro* crystallization experiment support this assumption. Only dish-like calcium carbonate spherulites (~6 μm in diameter) are captured at 4 hr in the solution with Mg/Ca = 1 and ACCBP (Fig. 2 g&h). A broad peak at ~1085 cm^{-1} in the Raman spectrum confirms that these spherulites are ACC (Fig. 2i). Clearly, these ACC spherulites are the precursors for aragonite or calcite particles at 24 hr.

To confirm that ACCBP induces the transformation from ACC precursor to aragonite, an ACC transformation experiment is conducted (Fig. 3). The samples collected at 0, 12, 24, 48, and 72 hr are analysed by FTIR. ACC is identified by a broad absorption band at ~866 cm^{-1} (ν2), aragonite by absorption bands at ~856 cm^{-1} (ν2), 713 cm^{-1} (ν4) and 700 cm^{-1} (ν4) (a weak band), and calcite by absorption bands at ~874 cm^{-1} (ν2) and ~713 cm^{-1} (ν4).[52] The results show that all the precipitates at 0 hr are ACC (Fig. 3). In the solution with Mg/Ca = 1, a strong absorption is observed for calcite at ~874 cm^{-1}, and the peak for ACC at ~866 cm^{-1} decreases at 12 hr; over time, the 874 cm^{-1}/866 cm^{-1} intensity ratio continuously increases, and the peak at ~866 cm^{-1} eventually disappears (Fig. 3a). These results suggest that the entire ACC is consumed to form calcite in the control experiment. In the solution with Mg/Ca = 1 and ACCBP, strong absorption at ~874 cm^{-1} and a small shoulder peak at ~856 cm^{-1} are observed at 12 hr; the 874 cm^{-1}/866 cm^{-1} intensity ratio increases over time, and the absorption at ~856 cm^{-1} changes slightly (Fig. 3b). Most of the ACC is again consumed to form calcite, but a small amount of aragonite is also induced by ACCBP. In the solution with Mg/Ca = 2, strong absorption at ~874 cm^{-1} is observed at 12 hr; a weak peak characteristic of aragonite at 856 cm^{-1} appears at 48 hr; and

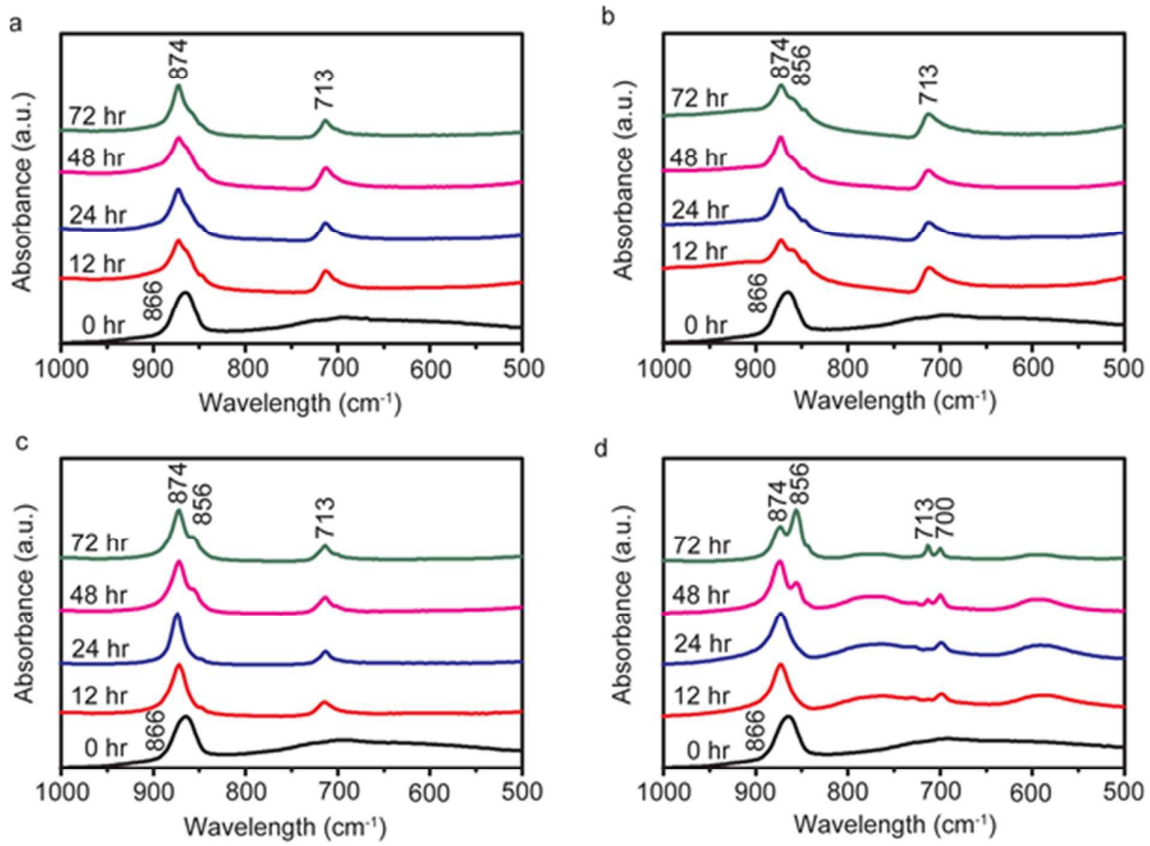

Fig. 3 FTIR analysis of the precipitates in the ACC transformation experiment. FTIR of the precipitates collected at different times from the mixed solutions with a) Mg/Ca = 1, b) Mg/Ca = 1 and 0.5 μM ACCBP, c) Mg/Ca = 2, d) Mg/Ca = 2 and 0.5 μM ACCBP.

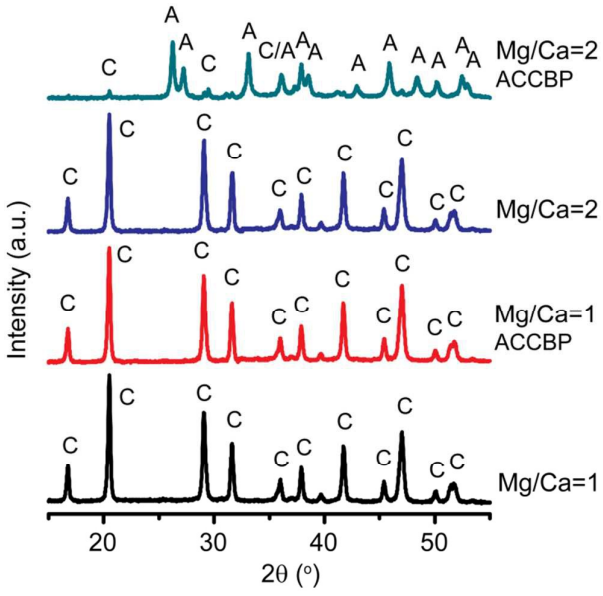

Fig. 4 XRD spectra of the final precipitates in the ACC transformation experiment. A: aragonite; C: calcite.

the 856 cm^{-1}/874 cm^{-1} intensity ratio does not change between 48 hr and 72 hr (Fig. 3c). Most of the ACC transforms into calcite, and a small proportion of the final mixture is aragonite. In the solution with Mg/Ca = 2 and ACCBP, the peak at ~874 cm^{-1} is broader at 12 and 24 hr than that without ACCBP, implying that ACC is more stable in the presence of ACCBP. The 856 cm^{-1}/874 cm^{-1} intensity ratio markedly increases at 48 hr, suggesting that a large amount of aragonite forms at this stage. The 856 cm^{-1}/874 cm^{-1} intensity ratio increases continuously up to 72 hr, suggesting that aragonite forms continuously, and most of the final product is aragonite (Fig. 3d). ACC is consumed to form aragonite in the presence of ACCBP in Mg/Ca = 2 solution.

The final precipitates collected on the 4th day of the ACC transformation experiment are analysed by XRD. In the solution with Mg/Ca = 1 and ACCBP, the calcite content of the final precipitates is greater than 95%, the same as the control group (Fig. 4). The results indicate that ACCBP induces only a small amount of aragonite formation in Mg/Ca = 1 solution. In the solution with Mg/Ca = 2 and ACCBP, more than 87% of the final product is aragonite, while more than 90% of the final product is still calcite in the control group, which shows that ACCBP induces aragonites in ACC transformation experiment. In the ACC transformation experiment II, ACC is synthesized

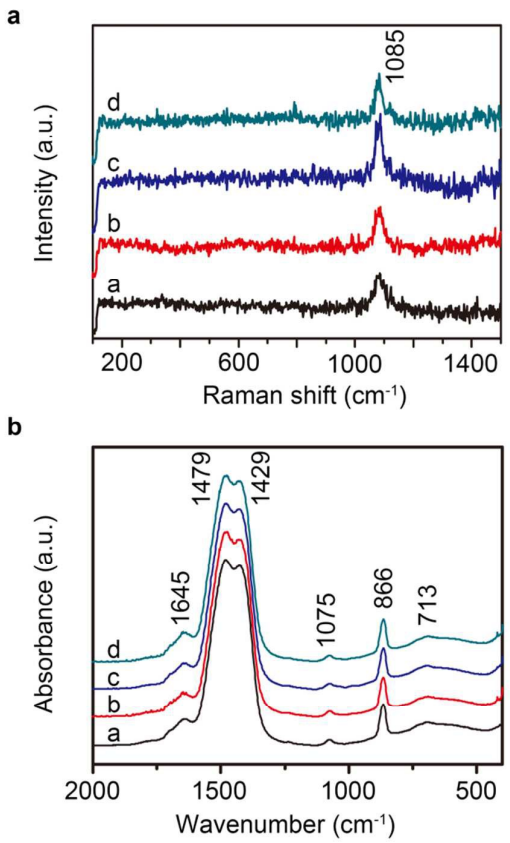

Fig. 5 Raman spectra a) and FTIR spectra b) of the initial-stage precipitates in the ACC transformation experiment. The precipitates are prepared in the following solution conditions: a) Mg/Ca = 1, b) Mg/Ca = 1 and 0.5 μM ACCBP, c) Mg/Ca = 2, d) Mg/Ca = 2 and 0.5 μM ACCBP.

first without ACCBP or Mg^{2+}, separated from the initial solution via centrifugation, and then resuspended in the solution with Mg/Ca = 1, 2, or 5, and with or without ACCBP (Fig. S3). The XRD analysis shows that ACCBP induces aragonite in solution with Mg/Ca = 5, while no aragonite is detected in the control experiment. The result confirms again that ACCBP induces aragonite with the help of Mg^{2+}.

Mg/Ca ratio on the initial-stage ACC surface is controlled by ACCBP. To understand how ACCBP induces aragonite formation via ACC precursor in solutions with low Mg^{2+} concentrations, the initial ACC precipitates collected at 0 hr in the ACC transformation experiment are analysed.

SEM images show that all the ACC samples consist of spherulites with diameters of 20-100 nm (Fig. S2). ACCBP does not seem to regulate the size or morphology of ACC at any Mg/Ca ratio. Raman spectra with only a broad peak at ~1085 cm^{-1} confirm that all the samples are ACC (Fig. 5a). The peaks at ~1085 cm^{-1} in all spectra are the same, and no discrete peak is found in the range of 100-300 cm^{-1} even though each spectrum profile represents the average of 10 separate scans. These practically identical spectra suggest that no structural

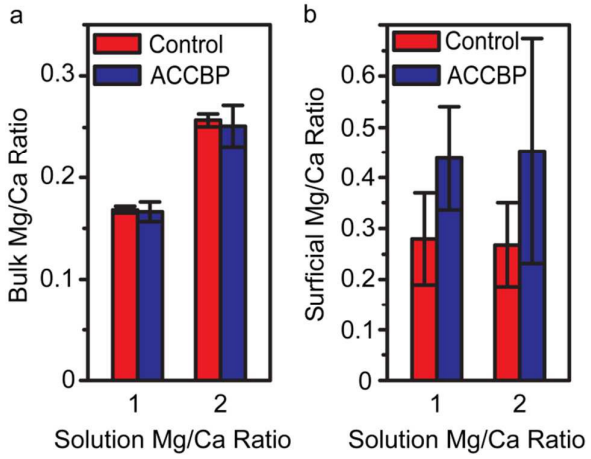

Fig. 6 Elemental analysis of the initial-stage precipitates in the ACC transformation experiment. a) Bulk Mg/Ca ratio of ACC analyzed by ICP. b) Surface Mg/Ca ratio of ACC analyzed by XPS.

difference is detected by Raman spectroscopy. The FTIR spectra confirm that all the samples are ACC by the split peaks at ~1429 and ~1479 cm^{-1} (ν3) (representing the asymmetric stretch of the carbonate ion), the broad and weak peak at ~1074 cm^{-1} (ν1) (representing the symmetric stretch in non-centrosymmetric structures), the peak at ~866 cm^{-1} (ν2) (representing the out-of-plane bending), and a weak and broad peak at ~713 cm^{-1} (ν4) (representing the in-plane bending) (Fig. 5b). The peak at ~866 cm^{-1}, the split peaks at ~1429 and ~1479 cm^{-1} and the intensity ratio of 866 cm^{-1}/713 cm^{-1} are not influenced by ACCBP. The practically identical FTIR spectra suggest that the local environment of the carbonate group in ACC are the same, implying that the local atomic orders of ACC samples are the same.[55] It is unlikely that ACCBP induces aragonite formation by regulating the short-range order structure of the initial-stage ACC. The conclusion is consistent with recent report that the amorphous phase precursor for abalone nacre is not proto-aragonite or poorly crystalline aragonite.[56]

ACCBP contains 11.11% Asp residues, and Asp acid can increase the Mg^{2+} content of ACC.[57] Therefore, it is supposed that ACCBP could affect the magnesium content of ACC. To test the hypothesis, the bulk Mg/Ca ratio of ACC is analysed by ICP. In the solution with Mg/Ca = 1 and ACCBP, the ratio is 0.166±0.007, similar to the control value of 0.171±0.002. In the solution with Mg/Ca = 2 and ACCBP, the ratio is 0.251±0.021, similar to the control value of 0.257±0.006 (Fig. 6a). ACCBP cannot regulate the bulk Mg/Ca ratio of ACC. The Mg/Ca ratio on the ACC surface is further analysed by XPS. In the solution with Mg/Ca = 1 and ACCBP, the ratio is 0.44±0.10, compared to 0.28±0.09 for the control. In the solution with Mg/Ca = 2 and ACCBP, the ratio is 0.45±0.22, compared to 0.27±0.08 for the control (Fig. 6b). This trend is always the same in the three independent experiments. XPS shows that ACCBP may increase the surface Mg/Ca ratio. Considering the Mg^{2+} effects

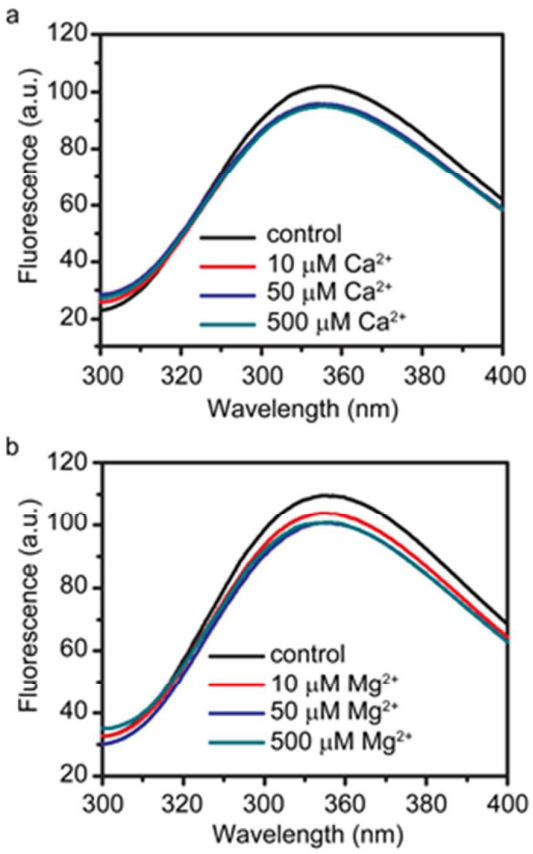

Fig. 7 Fluorescence quenching experiment. a) Intrinsic fluorescence of 5 μM ACCBP titrated with 10, 50, or 500 μM Ca^{2+}. b) Intrinsic fluorescence of 5 μM ACCBP titrated with 10, 50, or 500 μM Mg^{2+}.

in crystallization, ACCBP may control the polymorph switching by regulating the local Mg^{2+} content on the surface of ACC.

To confirm that ACCBP can increase the surface Mg/Ca ratio of ACC, a set of fluorescence quenching experiments are conducted. Addition of 10 μM Ca^{2+} quenches the intrinsic tryptophan fluorescence by 6% (Fig. 7a), almost the same level of quenching induced by 50 or 500 μM Ca^{2+}. Suppose it is static quenching, then the binding constant should be equal to the quenching constant. The binding constant for Ca^{2+} would be greater than 6.4×10^3 L/mol according to the Stern-Volmer relationship,[58] suggesting that Ca^{2+} is able to bind to ACCBP. This is consistent with that ACCBP can bind the surface of ACC and calcite. Addition of 10, 50 or 500 μM Mg^{2+} quenches intrinsic fluorescence by 5%, 8% or 8%, respectively (Fig. 7b), suggesting that the binding constant for Mg^{2+} is greater than 1.7×10^3 L/mol. The fact that ACCBP binds both Ca^{2+} and Mg^{2+} confirms that ACCBP may recruit Mg^{2+} onto the surface of ACC.

Discussion

To the best of our knowledge, this study is the first report of aragonite formation in the presence of an EPF protein. There are few researches concerning the functions of proteins from EPF, blood and mantle,[35, 38, 59-61] where ACC precursor is synthesized, stored and transported.[62-64] In the previous reports, these proteins are suggested to be involved in biomineralization. However, their functions in ACC formation and transformation remain unclear.

ACC is arguably important to the crystallization processes since it's the precursor of the other crystalline phases.[18] ACC nanoparticles will crystallize, assemble, and merge into platelets during nacre formation.[56, 65] Transformation of ACC can follow the sequence: hydrated ACC → anhydrous ACC → aragonite or calcite.[56, 66] Little is known about the formation of biogenic anhydrous ACC *in vivo*. ACCBP is involved in ACC stabilization and formation.[35, 37] FTIR and TGA results further show that ACCBP can decrease the water content of ACC from 1.0 to 0.82 mol of water per mol of calcium carbonate. SEM images of *in vitro* crystallization experiment show that ACC persists for more than 24 hours in presence of only ACCBP, and transforms into crystalline phase in 24 hours in presence of both ACCBP and Mg^{2+}. ACC is more unstable in presence of both ACCBP and Mg^{2+}. Macromolecules together with Mg^{2+} may mediate the biogenic anhydrous formation of ACC as a precursor to calcite.[15] Considering that Asp-rich proteins may destabilize the Mg^{2+}-stabilized ACC *in vivo*,[19] ACCBP may be involved in formation of biogenic anhydrous ACC in cooperation with Mg^{2+}.

An ACC transformation experiment in the presence of different concentrations of Mg^{2+} has been carried out at room temperature by Meldrum *et al*. years ago.[14] In Mg/Ca = 1 solution, the precipitation is observed immediately and the final product is principally calcite containing only a few percentage of vaterite; In Mg/Ca = 2 solution, ACC is identified in the initial stage and it transforms into calcite which sometimes contains trace quantities of aragonite; In Mg/Ca = 4 solution, the initial-stage ACC transforms into a mixture of 50% aragonite and 50% magnesian calcite at 48 hr and nesquehonite at 72 hr. These results are similar to that of our control experiments. In ACC transformation experiment, trace aragonite is found in the solution with ACCBP and Mg/Ca = 1, while no aragonite is detected by both FTIR and XRD in the control experiment. More than 87% of the final product is aragonite in the solution with ACCBP and Mg/Ca = 2, while only trace aragonite is detected by FTIR in the control experiment. This experiment is conducted at a temperature below 6°C. The control result is consistent with previous report that calcite is favored in low-Mg/Ca solution at this temperature.[53] Clearly, ACCBP induces aragonite formation in cooperation with Mg^{2+} in low Mg/Ca solutions. This conclusion is consistent with the recent report that organic matrix can promote aragonite formation in cooperation with Mg^{2+}.[67, 68]

Then, an interesting question comes up: How does ACCBP, an EPF protein, participate in the polymorph selection? According to the classical epitaxial match theory, ACCBP would control the ACC transformation by forming a nucleating template. However, the nucleating template does not occur in

our case. Oligomeric analysis and homology modelling show that the potential Ca^{2+}-binding sites of ACCBP are arranged in a five-fold symmetry pattern which hardly serves as a nucleating template for aragonite with an orthorhombic symmetry.[37] It is consistent with the result that ACCBP induces ACC in solution without any additive. ACCBP does not form a nucleating template in the presence of Mg^{2+} either. If we assume that Mg^{2+} would change the conformation of ACCBP to form a nucleation template for aragonite in the solution with Mg/Ca = 1, the number of templates should be the same in both the solution with Mg/Ca = 1 and ACCBP and the solution with Mg/Ca = 2 and ACCBP because of the same concentration of ACCBP. Keeping the same assumption, the aragonite content of the final product from the solution with Mg/Ca = 1 and ACCBP would also be the same as that from the solution with Mg/Ca = 2 and ACCBP in the ACC transformation experiment. However, the aragonite content of the final product from the solution with Mg/Ca = 1 and ACCBP is much less than that from the solution with Mg/Ca = 2 and ACCBP. If we assume that the concentration of Mg^{2+} is not enough to change the conformation of ACCBP to form a template in the solution with Mg/Ca = 1, there should be no template for aragonite in the solution with Mg/Ca = 1 and ACCBP. Keeping the same assumption, there should be no aragonite in the final product from the solution with Mg/Ca = 1 and ACCBP. However, trace aragonite is detected by FTIR and XRD in the product from the solution with Mg/Ca = 1 and ACCBP. Furthermore, FTIR and Raman analyses imply that the local atomic structure of ACC may not be regulated by ACCBP significantly. Thus, ACCBP cannot serve as a nucleating template for aragonite in solution with or without Mg^{2+}.

The question is now changed into how ACCBP controls the polymorph selection without a nucleating template. Elemental analyses indicate that ACCBP increases Mg/Ca ratio on surface of ACC without affecting the bulk Mg/Ca ratio. Carboxylated molecules increase the bulk Mg/Ca ratio of ACC and this ACC with increased bulk Mg/Ca ratio finally transforms into calcite.[57] ACCBP, a carboxylated protein, does not regulate the bulk Mg/Ca ratio. This may be because that the concentration of ACCBP is only one-thousandth of that of carboxylated organic acids used in the experiments. Then, the difference of surface Mg/Ca ratio may be the key for the polymorph selection. Mg^{2+} adsorption onto the surface of growing calcite crystals, slow dehydration of the Mg^{2+} ions prior to incorporation in the calcite lattice, and enhanced mineral solubility associated with Mg^{2+} incorporation would inhibit the calcite growth and then promote the aragonite formation.[53, 69, 70] The ACC-to-crystalline phase transformation may occur through dissolution and reprecipitation.[71, 72] ACC dissolve partly during this process,[73] the local Mg^{2+} will be higher because of the higher surface Mg/Ca ratio. Thus, ACCBP may induce aragonite formation by increasing Mg/Ca ratio on the ACC surface.

The epitaxial match theory is an excellent hypothesis interpreting the polymorph selection of calcium carbonate biominerals.[20] The template for epitaxial match locates on the surface of shell matrix.[21] Our data suggest that the

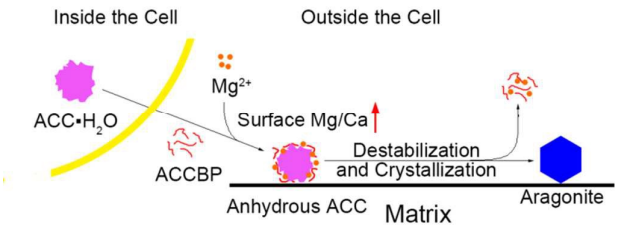

Fig. 8 Schematic representation of the suggested model for the polymorph selection controlled by ACCBP.

physicochemical effects of EPF protein may change the local environment on the surface of ACC nanoparticles, and that EPF protein may be involved in the polymorph selection during the amorphous-crystal transformation. This supposition may work with the classical epitaxial match to control the polymorph selection during shell formation.

By Combining the functions of ACCBP with its tissue distribution, a scenario for nacre growth is proposed (Fig. 8). Hydrated ACC nanograin forms by the aggregation of prenucleation ion clusters in vesicles. The hydrated ACC nanograin is immediately stabilized by Mg^{2+}, biomolecules or vesicles lipid membrane. When the hydrated ACC is transported into the mineralization site, it is dehydrated and transformed into aragonite under the control of ACCBP and Mg^{2+}. When the crystallization completes, ACCBP is excluded into EPF where ACCBP would function as a safeguard molecule against undesired precipitation. This is consistent with that ACCBP binds onto inner surface of nacre but cannot be detected in nacre, and that ACCBP is most abundant in EPF.[35] Controlling the formation, stabilization and transformation of ACC by proteins on the surface of individual ACC nanograin would be more convenient and efficient for the organisms. In this way, there is no need to synthesize different forms of ACC precursors because changing the conditions on the surface of ACC would conveniently switch the polymorph of the final product, and the proteins on the surface of the ACC could be recycled after the ACC has transformed into the crystalline phase.

Conclusions

In summary, we report that ACCBP, an EPF protein involved in ACC formation and stabilization, induces aragonite formation via ACC precursor in low Mg/Ca solution at low temperature. This polymorph switching may be controlled by increasing the surface Mg/Ca ratio of the ACC. Besides, ACCBP may be involved in the formation of biogenic anhydrous ACC in cooperation with Mg^{2+}. In addition to the classical epitaxial theory, this work provides a novel mechanism for polymorph selection via anhydrous amorphous phase precursors under the control of biomolecules. It highlights the physicochemical effects of EPF proteins in the biomineralization process and would contribute to our understanding of the nacre or pearl formation.

Acknowledgements

This work is supported by the National Natural Science Foundation of China Grants 31172382 and 31372502.

References

1 X. Li, W.-C. Chang, Y. J. Chao, R. Wang and M. Chang, *Nano Letters*, 2004, **4**, 613-617.
2 M. Rousseau, E. Lopez, P. Stempfle, M. Brendle, L. Franke, A. Guette, R. Naslain and X. Bourrat, *Biomaterials*, 2005, **26**, 6254-6262.
3 L. Addadi, D. Joester, F. Nudelman and S. Weiner, *Chemistry*, 2006, **12**, 980-987.
4 A. Jackson, J. Vincent and R. Turner, *Proceedings of the Royal Society of London B: Biological Sciences*, 1988, **234**, 415-440.
5 P. J. Smeets, K. R. Cho, R. G. Kempen, N. A. Sommerdijk and J. J. De Yoreo, *Nat Mater*, 2015, **14**, 394-399.
6 E. Beniash, J. Aizenberg, L. Addadi and S. Weiner, *Proceedings of the Royal Society of London B: Biological Sciences*, 1997, **264**, 461-465.
7 I. M. Weiss, N. Tuross, L. Addadi and S. Weiner, *Journal of Experimental Zoology*, 2002, **293**, 478-491.
8 Y. Politi, T. Arad, E. Klein, S. Weiner and L. Addadi, *Science*, 2004, **306**, 1161-1164.
9 L. Gago-Duport, M. Briones, J. Rodriguez and B. Covelo, *Journal of structural biology*, 2008, **162**, 422-435.
10 D. E. Jacob, R. Wirth, A. L. Soldati, U. Wehrmeister and A. Schreiber, *J Struct Biol*, 2011, **173**, 241-249.
11 D. Gebauer, A. Volkel and H. Colfen, *Science*, 2008, **322**, 1819-1822.
12 E. M. Pouget, P. H. Bomans, J. A. Goos, P. M. Frederik, G. de With and N. A. Sommerdijk, *Science*, 2009, **323**, 1455-1458.
13 J. Aizenberg, G. Lambert, S. Weiner and L. Addadi, *J Am Chem Soc*, 2002, **124**, 32-39.
14 E. Loste, R. M. Wilson, R. Seshadri and F. C. Meldrum, *Journal of Crystal Growth*, 2003, **254**, 206-218.
15 S. Raz, P. Hamilton, F. Wilt, S. Weiner and L. Addadi, *Advanced Functional Materials*, 2003, **13**, 480-486.
16 A. Al‐Sawalmih, C. Li, S. Siegel, P. Fratzl and O. Paris, *Advanced Materials*, 2009, **21**, 4011-4015.
17 D. Ren, Q. Feng and X. Bourrat, *Micron*, 2011, **42**, 228-245.
18 S. Weiner and L. Addadi, *Annual Review of Materials Research*, 2011, **41**, 21-40.
19 J. Tao, D. Zhou, Z. Zhang, X. Xu and R. Tang, *Proceedings of the National Academy of Sciences*, 2009, **106**, 22096-22101.
20 S. Mann, B. Heywood, S. Rajam and V. Wade, in *Mechanisms and Phylogeny of Mineralization in Biological Systems*, Springer, 1991, pp. 47-55.
21 F. Nudelman, B. A. Gotliv, L. Addadi and S. Weiner, *J Struct Biol*, 2006, **153**, 176-187.
22 G. Falini, S. Albeck, S. Weiner and L. Addadi, *Science*, 1996, **271**, 67.
23 M. Suzuki, K. Saruwatari, T. Kogure, Y. Yamamoto, T. Nishimura, T. Kato and H. Nagasawa, *Science*, 2009, **325**, 1388-1390.
24 R. A. Metzler, J. S. Evans, C. E. Killian, D. Zhou, T. H. Churchill, N. P. Appathurai, S. N. Coppersmith and P. Gilbert, *Journal of the American Chemical Society*, 2010, **132**, 6329-6334.
25 H.-L. Liu, S.-F. Liu, Y.-J. Ge, J. Liu, X.-Y. Wang, L.-P. Xie, R.-Q. Zhang and Z. Wang, *Biochemistry*, 2007, **46**, 844-851.
26 Z. Yan, G. Jing, N. Gong, C. Li, Y. Zhou, L. Xie and R. Zhang, *Biomacromolecules*, 2007, **8**, 3597-3601.
27 F. F. Amos, E. Destine, C. B. Ponce and J. S. Evans, *Crystal Growth & Design*, 2010, **10**, 4211-4216.
28 F. F. Amos and J. S. Evans, *Biochemistry*, 2009, **48**, 1332-1339.
29 F. F. Amos, C. B. Ponce and J. S. Evans, *Biomacromolecules*, 2011, **12**, 1883-1890.
30 C. B. Ponce and J. S. Evans, *Crystal Growth & Design*, 2011, **11**, 4690-4696.
31 E. C. Keene, J. S. Evans and L. A. Estroff, *Crystal Growth & Design*, 2010, **10**, 1383-1389.
32 Z. Huang and G. Zhang, *Crystal Growth & Design*, 2012, **12**, 1816-1822.
33 N. Nassif, N. Pinna, N. Gehrke, M. Antonietti, C. Jäger and H. Cölfen, *Proceedings of the National Academy of Sciences of the United States of America*, 2005, **102**, 12653-12655.
34 X. Li and Z. Huang, *Physical review letters*, 2009, **102**, 075502.
35 Z. Ma, J. Huang, J. Sun, G. Wang, C. Li, L. Xie and R. Zhang, *Journal of Biological Chemistry*, 2007, **282**, 23253-23263.
36 L. Xiang, W. Kong, J. Su, J. Liang, G. Zhang, L. Xie and R. Zhang, 2014.
37 J. Su, X. Liang, Q. Zhou, G. Zhang, H. Wang, L. Xie and R. Zhang, *Biochemical Journal*, 2013, **453**, 179-186.
38 F. F. Amos, M. Ndao and J. S. Evans, *Biomacromolecules*, 2009, **10**, 3298-3305.
39 S. Liu, J. Su, J. Liu, J. Huang, D. Fang, L. Xie, H. Wang, G. Zhang, X. Du and C. Ma, *Journal of Guangdong Ocean University*, 2012, **3**, 003.
40 X. Liu, J. Li, L. Xiang, J. Sun, G. Zheng, G. Zhang, H. Wang, L. Xie and R. Zhang, *Proceedings of the Royal Society of London B: Biological Sciences*, 2012, **279**, 1000-1007.
41 L. Xiang, J. Su, G. Zheng, J. Liang, G. Zhang, H. Wang, L. Xie and R. Zhang, *PLoS One*, 2013, **8**, e66564.
42 J. Xie, J. Liang, J. Sun, J. Gao, S. Zhang, Y. Liu, L. Xie and R. Zhang, *Crystal Growth & Design*, 2015.
43 L. Addadi and S. Weiner, *Proceedings of the National Academy of Sciences*, 1985, **82**, 4110-4114.
44 G. Falini, S. Fermani, M. Gazzano and A. Ripamonti, *Journal of the Chemical Society, Dalton Transactions*, 2000, 3983-3987.
45 G. Xu, N. Yao, I. A. Aksay and J. T. Groves, *Journal of the American Chemical Society*, 1998, **120**, 11977-11985.
46 N. Koga, Y. Nakagoe and H. Tanaka, *Thermochimica Acta*, 1998, **318**, 239-244.
47 F. H. Chung, *Journal of Applied Crystallography*, 1974, **7**, 519-525.
48 M. Faatz, F. Gröhn and G. Wegner, *Advanced Materials*, 2004, **16**, 996-1000.
49 X.-R. Xu, A.-H. Cai, R. Liu, H.-H. Pan, R.-K. Tang and K. Cho, *Journal of Crystal Growth*, 2008, **310**, 3779-3787.
50 Y. Levi-Kalisman, S. Raz, S. Weiner, L. Addadi and I. Sagi, *Advanced Functional Materials*, 2002, **12**, 43-48.
51 C. Gabrielli, R. Jaouhari, S. Joiret and G. Maurin, *Journal of Raman Spectroscopy*, 2000, **31**, 497-501.

52 L. Addadi, S. Raz and S. Weiner, *Advanced Materials*, 2003, **15**, 959-970.
53 J. W. Morse, R. S. Arvidson and A. Lüttge, *Chemical reviews*, 2007, **107**, 342-381.
54 S. Raz, S. Weiner and L. Addadi, *Advanced Materials*, 2000, **12**, 38-42.
55 R. Gueta, A. Natan, L. Addadi, S. Weiner, K. Refson and L. Kronik, *Angewandte Chemie International Edition*, 2007, **46**, 291-294.
56 R. T. DeVol, C. Y. Sun, M. A. Marcus, S. N. Coppersmith, S. C. Myneni and P. U. Gilbert, *J Am Chem Soc*, 2015, **137**, 13325-13333.
57 D. Wang, A. F. Wallace, J. J. De Yoreo and P. M. Dove, *Proceedings of the National Academy of Sciences*, 2009, **106**, 21511-21516.
58 J. S. Johansson, *Journal of Biological Chemistry*, 1997, **272**, 17961-17965.
59 J. Huang, H. Wang, Y. Cui, G. Zhang, G. Zheng, S. Liu, L. Xie and R. Zhang, *Marine biotechnology*, 2009, **11**, 596-607.
60 S. J. Hattan, T. M. Laue and N. D. Chasteen, *Journal of Biological Chemistry*, 2001, **276**, 4461-4468.
61 Y. Yin, J. Huang, M. L. Paine, V. N. Reinhold and N. D. Chasteen, *Biochemistry*, 2005, **44**, 10720-10731.
62 J. M. Neff, *Tissue and Cell*, 1972, **4**, 591-600.
63 A. S. Tompa and N. Watabe, *Calcified tissue research*, 1977, **22**, 159-172.
64 E. Beniash, L. Addadi and S. Weiner, *Journal of structural biology*, 1999, **125**, 50-62.
65 R. Hovden, S. E. Wolf, M. E. Holtz, F. Marin, D. A. Muller and L. A. Estroff, *Nature communications*, 2015, **6**.
66 Y. U. Gong, C. E. Killian, I. C. Olson, N. P. Appathurai, A. L. Amasino, M. C. Martin, L. J. Holt, F. H. Wilt and P. Gilbert, *Proceedings of the National Academy of Sciences*, 2012, **109**, 6088-6093.
67 D. Ren, Q. Feng and X. Bourrat, *Materials Science and Engineering: C*, 2013, **33**, 3440-3449.
68 Y. Ma and Q. Feng, *CrystEngComm*, 2015, **17**, 32-39.
69 A. Mucci and J. W. Morse, *Geochimica et Cosmochimica Acta*, 1983, **47**, 217-233.
70 K. J. Davis, P. M. Dove and J. J. De Yoreo, *Science*, 2000, **290**, 1134-1137.
71 P. Bots, L. G. Benning, J.-D. Rodriguez-Blanco, T. Roncal-Herrero and S. Shaw, *Crystal Growth & Design*, 2012, **12**, 3806-3814.
72 C. Rodriguez-Navarro, K. Kudłacz, Ö. Cizer and E. Ruiz-Agudo, *CrystEngComm*, 2015, **17**, 58-72.
73 Z. Zhang, Y. Xie, X. Xu, H. Pan and R. Tang, *Journal of Crystal Growth*, 2012, **343**, 62-67.